Extrahepatic PPARα modulates fatty acid oxidation and attenuates fasting-induced hepatosteatosis in mice[S]

Chad N. Brocker,[1] Daxesh P. Patel,[1] Thomas J. Velenosi, Donghwan Kim, Tingting Yan, Jiang Yue,[2] Guolin Li,[3] Kristopher W. Krausz, and Frank J. Gonzalez[4]

Laboratory of Metabolism, Center for Cancer Research, National Cancer Institute, National Institutes of Health, Bethesda, MD 20892

Abstract **PPARα (PPARA), expressed in most oxidative tissues, is a major regulator of lipid homeostasis; hepatic PPARA plays a critical role during the adaptive fasting response by promoting FA oxidation (FAO). To clarify whether extrahepatic PPARA activity can protect against lipid overload when hepatic PPARA is impaired, lipid accumulation was compared in WT (*Ppara*$^{+/+}$), total body *Ppara*-null (*Ppara*$^{-/-}$), and hepatocyte-specific *Ppara*-null (*Ppara*$^{\Delta Hep}$) mice that were fasted for 24 h. Histologic staining indicated reduced lipid accumulation in *Ppara*$^{\Delta Hep}$ versus *Ppara*$^{-/-}$ mice, and biochemical analyses revealed diminished medium- and long-chain FA accumulation in *Ppara*$^{\Delta Hep}$ mouse livers. Hepatic PPARA target genes were suppressed in both mouse models. Serum FFAs increased in all genotypes after fasting but were highest in *Ppara*$^{-/-}$ mice. In *Ppara*$^{\Delta Hep}$ mice, FAO genes were increased in brown adipose tissue, heart, and muscle, and total lipase activity was elevated in the muscle and heart, suggesting increased lipid utilization. Thus, extrahepatic PPARA activity reduces systemic lipid load when hepatic lipid metabolism is impaired by elevating FAO and lipase activity in other tissues and, as a result, protects against fasting-induced hepatosteatosis. This has important clinical implications in disease states with impaired hepatic PPARA function, such as nonalcoholic steatohepatitis and nonalcoholic fatty liver disease.**—Brocker, C. N., D. P. Patel, T. J. Velenosi, D. Kim, T. Yan, J. Yue, G. Li, K. W. Krausz, and F. J. Gonzalez. **Extrahepatic PPARα modulates fatty acid oxidation and attenuates fasting-induced hepatosteatosis in mice. *J. Lipid Res.* 2018.** 59: **2140–2152**.

Supplementary key words nuclear receptors • lipase • caloric restriction • peroxisome proliferator-activated receptor

PPARα (PPARA) is considered a major regulator of systemic lipid homeostasis and, consequently, the prolonged fasting response. PPARA is a ligand-activated nuclear receptor that modulates transcription of specific target genes involved in lipid oxidation, lipid transport, lipoprotein assembly, and ketogenesis. During fasting, hepatic PPARA acts as a nutrient sensor and responds to the influx of lipid by upregulating target genes associated with lipid catabolism and ketone body (KB) synthesis to ensure energy availability for extrahepatic tissues. Studies in *Ppara*-null mice (*Ppara*$^{-/-}$) confirmed a critical role for PPARA during prolonged fasting and starvation. These mice experience hepatic lipid accumulation that manifests as pronounced steatosis (1–3). Fasted *Ppara*$^{-/-}$ mice also develop hypoketonemia, hypoglycemia, and hypothermia. Hepatic PPARA deficiency is thus a major contributing factor to the observed phenotype. Because PPARA is highly expressed in the liver, the majority of studies have focused on hepatic PPARA action. Nevertheless, PPARA is expressed in most oxidative tissues, including heart, muscle, and kidney, as well as brown adipose tissue (BAT), and activation of extrahepatic PPARA may contribute significantly to lipid homeostasis in response to prolonged fasting.

Fasting causes a decrease in blood glucose (GLU) levels and triggers glucagon release from the pancreas. Glucagon

This work was funded by the intramural research program at the National Cancer Institute. C.N.B. was supported by the Postdoctoral Research Associate Training program through the National Institute of General Medical Sciences. The content is solely the responsibility of the authors and does not necessarily represent the official views of the National Institutes of Health.

Manuscript received 10 July 2018 and in revised form 22 August 2018.

Published, JLR Papers in Press, August 29, 2018
DOI https://doi.org/10.1194/jlr.M088419

Abbreviations: Acadm, acyl-CoA dehydrogenase, medium chain; Acadl, acyl-CoA dehydrogenase, long chain; Actb, β-actin; a.k.a., also known as; ALT, alanine aminotransferase; AST, aspartate aminotransferase; BAT, brown adipose tissue; CHOL, cholesterol; Cpt1b, carnitine palmitoyltransferase 1b; CR, caloric restriction; Cyp2b9, cytochrome P450, family 2, subfamily b, polypeptide 9; Cyp8b1, cytochrome P450, family 8, subfamily b, polypeptide 1; Ehhadh, enoyl-CoA hydratase and 3-hydroxyacyl CoA dehydrogenase; Etnppl, ethanolamine-phosphate phospho-lyase; EWAT, epididymal white adipose tissue; FAO, FA oxidation; Fgf21, fibroblast growth factor 21; GLU, glucose; IWAT, inguinal white adipose tissue; KB, ketone body; LCFA, long-chain FA; Lcn, lipocalin; Lcn2, lipocalin 2; Lcn13, lipocalin 13; LPO, lipid peroxidation; MCFA, medium-chain FA; MSD, mass-selective detector; NASH, nonalcoholic steatohepatitis; NAFLD, nonalcoholic fatty liver disease; ORO, Oil red O; Pdk4, pyruvate dehydrogenase kinase 4; PL, phospholipid; PPARA, PPARα; qRT-PCR, quantitative RT-PCR; ROS, reactive oxygen species; TG, triglyceride.

[1] C. N. Brocker and D. P. Patel contributed equally to this work.
[2] Present address: Department of Pharmacology, School of Medicine, Wuhan University, Wuhan 430071, China.
[3] Present address: Laboratory of Aging Biochemistry, College of Life Sciences, Hunan Normal University, Changsha 410081, China.[4] To whom correspondence should be addressed.
email: gonzalef@mail.nih.gov

[S] The online version of this article (available at http://www.jlr.org) contains a supplement.

elicits a wide range of metabolic alterations, primarily within the liver, to restore energy homeostasis. Hepatic glycogenolysis mobilizes GLU from glycogen stores. Gluconeogenesis also generates GLU from noncarbohydrate sources, including lactate and glycerol (GLY). Prolonged fasting initiates a gradual shift from utilizing carbohydrates and lipids in the fed state to predominantly FAs as GLU stores become exhausted. The shift to lipids as a primary energy source is dependent on the mobilization of FFAs from adipose tissue and circulating lipoproteins. FFAs released from adipose tissue are transported as NEFAs bound to serum albumin. Esterified FAs are transported within circulating lipoproteins. FA uptake by tissues primarily occurs through LPL- or CD36-mediated pathways. LPL hydrolyzes triglyceride (TG)-containing lipoproteins, whereas CD36 acts as a FA translocase to transfer albumin-bound FAs into tissues. Fasting-induced FA influx into oxidative tissues such as the liver, muscle, and heart subsequently activates PPARA, stimulating target gene activation and lipid catabolism.

A growing body of evidence indicates that fasting and caloric restriction (CR) imbue many beneficial outcomes, including reduced fat mass, increased insulin sensitivity, reduced cancer prevalence, delayed neurodegeneration, increased longevity, and improved overall health (4). Fasting causes FA uptake into many PPARA-expressing tissues. Therefore, it is reasonable to assume that PPARA action in extrahepatic tissues significantly contributes to systemic lipid homeostasis during food deprivation. Understanding the underlying mechanisms that drive these metabolic alterations will aid in the development of novel therapeutics that mimic the beneficial effects of fasting or CR regimens. Moreover, hepatic PPARA expression and activity are suppressed in many disease states that cause lipid accumulation within the liver, including nonalcoholic steatohepatitis (NASH), nonalcoholic fatty liver disease (NAFLD), and hepatitis C infections (5–7). NASH and NAFLD patients also exhibit elevated total (esterified and free) FAs and FFAs in plasma, suggesting that PPARA agonism in these patient populations might be efficacious in reducing circulating FAs via extrahepatic PPARA pathways (8, 9). PPARA expression is high in the liver, and fasting studies have focused on PPARA action within this tissue. Less is known about its function in extrahepatic tissues or the overall contribution of extrahepatic PPARA activation to systemic lipid metabolism. More recently, studies have shown that PPARA expression levels within oxidative tissues—namely, liver, heart, kidney, and skeletal muscle—are comparable, highlighting how PPARA is functionally important in several tissues, not just the liver (10, 11). In addition, studies have noted that relative *Ppara* mRNA expression levels in various tissues are similar between mice and humans (10). The development of tissue-specific *Ppara*-null mice makes it possible to directly assess the contribution of extrahepatic tissues to systemic lipid homeostasis. This study tested the hypothesis that extrahepatic PPARA plays a significant role during metabolic response to fasting and that PPARA activity in nonhepatic tissues can attenuate hepatosteatosis when liver PPARA signaling is impaired.

METHODS

Animal care and treatment

Ppara WT ($Ppara^{+/+}$) and $Ppara^{-/-}$ mice used in this study were described previously (12). Floxed *Ppara* ($Ppara^{F/F}$) and hepatocyte-specific *Ppara*-null ($Ppara^{\Delta Hep}$) mice were generated as described previously (13). Groups of $Ppara^{+/+}$ and $Ppara^{F/F}$ mice were included in all experiments. Physiological response between the two control mouse strains—namely, WT and floxed—were statistically identical. Data from only the $Ppara^{+/+}$ mice were presented to simplify data interpretation and figure clarity. Mice from each genotype were on the C57BL/6J background and used at 8–10 weeks of age. A breeding strategy was established to reduce genetic drift between mouse lines. Homozygous breeder cages for experimental animals were created using pups from heterozygous crosses between $Ppara^{+/-}$ or $Ppara^{F/+}$ mice. Heterozygous breeder cages were in turn set up using homozygous $Ppara^{-/-}$ or $Ppara^{F/F}$ mice crossed with a C57BL/6J mouse. This breeding strategy ensures that the background of all the genetically modified mice are constantly being backcrossed into the original C57BL/6J line. Mice were maintained on a grain-based control diet (NIH-31). For fasting studies, food was removed for 24 h starting shortly after the onset of the light cycle (ZT4) and endpoints collected at the same time the following day. Body composition analysis for total body fat and lean mass were determined using an EchoMRI 3-in-1 mouse scanner (EchoMRI, Houston, TX) on nonanesthetized live mice following manufacturer's protocol. Body temperatures were measured rectally using a TH-5 Thermalert Monitoring Thermometer coupled to a RET-3 rectal probe lubricated with mineral oil inserted to a marked depth of 1.9 cm (Physitemp, Clifton, NJ). Animals were then euthanized by CO_2 asphyxiation, and tissue samples were collected for further analysis. Blood was collected by venipucture of the caudal vena cava. All mice were housed in a temperature- and light-controlled vivarium and given food and water ad libitum. All mouse studies were carried out in accordance with protocols approved by the National Cancer Institute Animal Care and Use Committee.

Histological staining

Fresh liver tissue was immediately fixed in 10% phosphate-buffered formalin for 24 h and then processed in paraffin blocks. Four-micrometer sections were used for H&E staining. For Oil Red O (ORO) staining, fresh liver tissue was placed into a cryomold and filled with OCT Compound (Tissue-Tek), then transferred to a beaker of isopentane prechilled in liquid nitrogen. Sections were processed by HistoServ, Inc. (Germantown, MD). Slide imaging was performed using a Keyence BZ-X700 series all-in-one microscope with both 20× and 40× objectives, 200× and 400× magnification, respectively.

Sample preparation for analyte analysis by GC/MS

Total FAs were measured in liver tissue after acid hydrolysis. In short, livers were removed, and 20 mg of liver tissue was placed in 0.5 ml of myristic acid-d27 (IS, 20 μM) in dichloromethane, and then 0.5 ml of 70% acetonitrile in water was added, followed by homogenization using a Precellys homogenizer and 1 mm zirconia/silica beads for 30 s at 6,000 *g*. The samples were centrifuged at 20,000 *g* for 10 min at 4°C. The lower organic layer (0.4 ml) was transferred to a glass tube and dried down in a SpeedVac concentrator at room temperature. The resulting dried residue was dissolved in 0.3 ml of 1.25 M HCl in methanol and then incubated for 1 h at 100°C. Then, 0.4 ml of n-hexane was added to each tube, samples were vortexed for 1 min, and 1 μl of each sample was injected into the chromatographic system for analysis as described below.

Samples for GLY measurements were prepared as follows. Twenty microliters of 10 μM DL-norleucine was added to 50 μl of mouse serum. Samples were vortexed for 10 s, and 0.6 ml of acetonitrile was added, then vortexed for another minute. The samples were centrifuged at 20,000 *g* for 15 min at 4°C, and 530 μl of supernatant was transferred to 2 ml vials. Samples were dried in a SpeedVac concentrator at room temperature. The dried residue was derivatized by adding 50 μl of *N*-trimethylsilylimidazole and sonicated for 30 min at room temperature. The samples were diluted with 50 μl of acetonitrile and briefly vortexed for 10 s, and 1 μl was injected into the GC/MS system using an autosampler. Calibration curve standards were made at 2, 5, 10, 25, 50, 100, and 200 μM GLY for absolute quantification. Linear regression with weighting factor of $1/x^2$ was used to represent peak area ratio (analyte/IS) response obtained through single ion monitoring versus concentration plot with a correlation coefficient of ⩾0.99 for GLY.

Chromatographic and mass detection parameters for GC/MS analysis

All FA analytes were separated on a capillary column (30 m × 0.250 mm, 0.25 μm; Agilent Technologies, Foster City, CA). Analyses were performed with an Agilent 6890N gas chromatograph coupled to an Agilent 5973 mass-selective detector (MSD) with the following chromatographic conditions: initial temperature 60°C for 2 min, increasing to 150°C at 20°C/min over 6.5 min and finally to 300°C at 7.5°C/min with 1.0 min hold time for total 27.5 min run time. The front inlet temperature was 250°C operating with a split ratio of 1:25. MSD ion source and interface temperatures were 230°C and 280°C, respectively. Oven temperature and AUX-2 temp were set at 60°C and 280°C. The MSD operated in EI mode at 70 eV. SIM mode of *m/z* 20–650 was used for the analyses. Carrier gas was He (1.0 ml/min). GC/MS data were acquired and processed using Agilent MassHunter WorkStation software. GC/MS mass parameters can be found in supplemental Table S1.

GLY chromatography was carried out on a HP-5MS capillary column (30 m × 0.250 mm, 0.25 μm; Agilent Technologies) with 32.0 min run time and separated at 5.8 min retention time, *m/z* 205.2 (qualifier ions *m/z* 73.2, 103.1) TMS derivatives on SIM mode of *m/z* 30–650. Analyses were performed with an Agilent 6890N gas chromatograph coupled to an Agilent 5973 MSD with the following chromatographic conditions: Initial temperature 100°C for 2 min, increasing to 250°C at 10°C/min for 32 min. The front inlet temperature was 280°C operating with a split less mode. The MSD ion source and interface temperature was 230°C. The MSD was operated in EI mode at 70 eV. Carrier gas was He (1.5 ml/min). GCMS data were acquired and processed using Agilent MassHunter WorkStation software.

Serum biochemistry

Blood was collected from mice and transferred to BD Microtainer Serum Separator Tubes (Becton Dickinson, Franklin Lakes, NJ). Serum chemistry analysis for total cholesterol (CHOL), TG, phospholipids (PLs), total KBs, and NEFAs was performed using Wako Clinical Diagnostics kits (WakoUSA, Richmond, VA). Serum alanine aminotransferase (ALT) and aspartate aminotransferase (AST) levels were measured using Catachem VETSPEC Kits as recommended by the manufacturer (Catachem, Oxford, CT). Blood GLU levels were measured using a Contour blood GLU meter (Bayer, Mishawaka, IN).

Sample preparation for serum lipid analysis by LC/MS

For serum lipidomics analysis, 25 μl of serum was extracted by 4-fold cold chloroform:methanol (2:1) solution containing the following as internal standards: 2 μM lysophosphatidylcholine (17:0), phosphatidylcholine (17:0), sphingomyelin (17:0), and ceramide (17:0; Avanti Polar Lipids, Alabaster, AL). The samples were vortexed for 30 s and then allowed to stand for 5 min at room temperature. The mixture was centrifuged at 15,000 *g* for 5 min, and then the lower organic phase was collected and evaporated at room temperature under constant nitrogen gas stream, and the residue was dissolved in chloroform:methanol (1:1), followed by diluting with isopropanol:acetonitrile:H_2O (2:1:1) before LC/MS analysis.

Chromatographic and mass detection parameters for LC/MS analysis

For lipidomics discovery, samples were analyzed by ultraperformance LC (UPLC)-ESI-quadrupole TOFMS using a Waters Acquity CSH 1.7 μm C18 column (2.1 × 100 mm) under the following conditions: UPLC: A: acetonitrile/water (60/40); B: isopropanol/acetonitrile (90/10), and both A and B contained 10 mM ammonium acetate and 0.1% formic acid. Gradient was initial 60% A to 57% A at 2 min, to 50% A at 2.1 min*, to 46% A at 12 min, to 30% A at 12.1 min*, to 1% A at 18 min, before returning to initial conditions at 18.5 min with equilibration for two additional minutes (where * indicates ballistic gradient). Flow rate was 0.4 ml/min. Column temperature was maintained at 55°C. MS was the same conditions as above, except run time was 18 min.

In vivo lipolysis assays by CL316243

Eight- to 10-week-old male *Ppara*$^{+/+}$, *Ppara*$^{-/-}$, and *Ppara*$^{\Delta Hep}$ mice were given an intraperitoneal injection of the β3-adrenoceptor agonist CL316243 (0.5 mg/kg) (Sigma-Aldrich, St. Louis, MO) or PBS as a vehicle control to assess adipose lipolysis. One hour postinjection, mice were euthanized by CO_2 asphyxiation, and blood was collected from the vena cava. As a measure of lipolysis, serum-free FAs and GLY were measured by LC/MS and GC/MS, respectively, as detailed above.

Gene expression analysis

Fifty milligrams of tissue was homogenized in TRIzol reagent (Thermo-Fisher, Waltham, MA) using a Percellys bead homogenizer (Bertin, Rockville, MD) and 1 mm zirconia/silica beads. Total RNA was isolated following manufacturer's guidelines and quantified using a NanoDrop spectrophotometer (NanoDrop Products, Wilmington, DE). Two micrograms of RNA was reverse transcribed with All-in-One cDNA Synthesis Super Mix (BioTool, Houston, TX) and used for quantitative RT-PCR (qRT-PCR) analysis with SYBR Green qPCR Master Mix (BioTool). Primers were designed for gene specificity and to cross exon-exon junctions using Primer-BLAST (www.ncbi.nlm.nih.gov/tools/primer-blast/) and purchased from IDT DNA Technologies (Coralville, IA). Results were normalized to β-actin (*Actb*) mRNA expression. qRT-PCR experiments were designed and performed according to Minimum Information for Publication of Quantitative Real-Time PCR Experiments guidelines (14). Values given are fold over control or relative expression value, where appropriate, calculated using the 2Δ*Ct* qPCR calculation method (15). Primer sequences can be found in supplemental Table S2.

Hepatic malondialdehyde and 2′,7′-dichlorofluorescin diacetate assays

Fresh liver tissue was homogenized and assayed for lipid peroxidation (LPO) and reactive oxygen species (ROS). LPO was measured using a Lipid Peroxidation Assay Kit (Abcam, Cambridge, UK) per the manufacturer's protocol. Cellular ROS was detected as previously described using a fluorescence probe. Briefly, 2',7'-dichlorofluorescin diacetate (DCFDA; final concentration 2.5 μM) was added to homogenates, and the changes in

fluorescence intensity were measured every 5 min for 30 min using a fluorescence plate reader (EnSpire Multimode Plate Reader, PerkinElmer, Waltham, MA) at excitation and emission wavelengths of 485 and 530 nm.

Tissue total lipase activity assays

Liver, heart, and skeletal muscle (soleus) were homogenized in ice-cold PBS buffer using a Percellys bead homogenizer and 1 mm zirconia/silica beads. Following homogenization, crude lysates were sonicated in a Diagenode Bioruptor Pico (Diagenode, Denville, NJ). Tissue total lipase activity was assayed using a fluorometric lipase activity assay kit (Abcam) following the manufacturer's recommendations and normalized to total protein. According to the manufacturer, assay specificity has been confirmed for LPL, hormone-sensitive lipase [also known as (a.k.a.) LIPE], hepatic TG lipase (a.k.a. LIPC), and pancreatic TG lipase (a.k.a. PNLIP). Adipose TG lipase (a.k.a. PNPLA2) activity should also be detectable, although specificity has not directly been confirmed. Protein concentrations were determined using a Pierce BCA Protein Assay Kit (Thermo-Fisher).

Statistical analysis

All results are expressed as the mean ± SD. Significance was determined by *t*-test or two-way ANOVA with Bonferroni posttest using Prism 6.0 software (GraphPad Software, La Jolla, CA). A P value of < 0.05 was considered significant and is indicated in graphs (* $P < 0.05$; ** $P < 0.01$; *** $P < 0.001$). Outliers were tested for using the Grubb's test statistic.

RESULTS

Extrahepatic PPARA activity attenuates hepatic lipid accumulation

To specifically assess the contribution of hepatocyte-specific *Ppara* disruption to the fasting phenotype, $Ppara^{+/+}$, $Ppara^{\Delta Hep}$, and $Ppara^{-/-}$ mice were fed al libitum or fasted for 24 h, then euthanized. Body weights for all genotypes decreased approximately 15% in response to fasting (**Fig. 1A**). Echo-MRI measurements of fed mice revealed that complete ablation of *Ppara* had resulted in significantly higher body fat composition when compared with either $Ppara^{+/+}$ or $Ppara^{\Delta Hep}$ mice (Fig. 1B, C) and that the weight loss in response to fasting did not affect relative percentages of lean or fat mass within each genotype. $Ppara^{-/-}$ mice also experienced fasting-induced hypothermia (Fig. 1D). Although the average fasted liver weights for $Ppara^{-/-}$ mice were slightly higher than $Ppara^{+/+}$ or $Ppara^{\Delta Hep}$ mice, the liver indices (mg liver/g body mass) between all groups were similar (Fig. 1E, F).

Gross liver morphology showed a much paler color in fasted $Ppara^{-/-}$ mice, indicative of lipid accumulation (**Fig. 2A**, upper) (3). Visual comparison of crude liver homogenates provided further support for differential lipid accumulation in the two mouse models (data not shown) and was confirmed using an enzymatic assay for TGs (Fig. 2B). Liver TGs accumulated in all groups in response to fasting. TG levels in $Ppara^{-/-}$ mice were elevated 2-fold over $Ppara^{+/+}$ mice and 30% higher than the $Ppara^{\Delta Hep}$ mice. H&E staining was used to assess tissue morphology and cell structure (Fig. 2C, D). Pronounced vacuole formation in fasted $Ppara^{-/-}$ mice were indicative of centrilobular steatosis. Vacuole accumulation was also observed in $Ppara^{\Delta Hep}$ mice, but to a lesser degree. H&E staining of ad libitum groups did not indicate any morphological differences between genotypes. ORO was used to stain for neutral lipids and cholesteryl esters (Fig. 2E). ORO staining confirmed differential lipid accumulation in fasted $Ppara^{-/-}$ and $Ppara^{\Delta Hep}$ mice. WT mice also exhibited a slight increase in hepatic lipid accumulation when compared with controls, but levels were significantly less than either knockout mouse model. The differential accumulation of lipids within the livers of hepatocyte-specific *Ppara*-null mice provides strong evidence that extrahepatic PPARA significantly contributes to systemic lipid homeostasis in response to CR.

Effect of fasting on hepatic FA composition

Total FA composition in livers was measured by GC/MS. *Ppara* ablation impacted the accumulation of saturated medium-chain FAs (MCFAs) (C10:0 and C12:0) and long-chain FAs (LCFAs) (C13:0, C14:0, C15:0, and C16:0) (**Fig. 3A**), monounsaturated LCFAs (C14:1, C16:1, C18:1, and C22:1) (Fig. 3B), and PUFAs (C18:2, C18:3, and C20:2) (Fig. 3C). PPARA expression in extrahepatic tissues protected against accumulation of many saturated (C14:0, C15:0, and C16:0) and unsaturated (C14:1, C16:1, C18:1, C22:1, and 20:2) FAs, which were significantly lower in $Ppara^{\Delta Hep}$ than $Ppara^{-/-}$ mice. Analysis revealed that hepatic and extrahepatic PPARA activity had less effect on accumulation of longer-chain PUFAs (Fig. 3C) and unsaturated LCFAs (Fig. 3D). FA species C20:1, C20:4, C20:5, C23:0, and C24:1 were slightly elevated in WT mice but unchanged in both mouse models, whereas PUFAs C18:3 and C22:6 increased in all groups after fasting.

Effect of fasting and extrahepatic PPARA on serum biochemistry

Serum chemistries were analyzed to assess the impact of extrahepatic PPARA activity on systemic lipid homeostasis. Hepatic steatosis impairs liver function and causes liver damage that is reflected in serum ALT and AST levels, which increased significantly in both mouse models after fasting (**Fig. 4A**, B). AST levels were lower in fasted $Ppara^{\Delta Hep}$ than $Ppara^{-/-}$ mice, indicating that liver damage was not as severe. Serum CHOL was slightly elevated in $Ppara^{\Delta Hep}$ mice but unaffected by fasting (Fig. 4C). All mice were hypoglycemic after a 24 h fast (Fig. 4D). However, hypoglycemia was more severe in fasted $Ppara^{-/-}$ mice followed by $Ppara^{\Delta Hep}$ then $Ppara^{+/+}$. Because PPARA acts as a major regulator of ketogenesis in the liver, total KBs were also measured (Fig. 4F). Serum KBs increased in all genotypes after fasting; however, KB response was diminished in both mouse models. NEFA levels were measured enzymatically and elevated in all genotypes (Fig. 4G). Fasting NEFAs were higher in $Ppara^{-/-}$ mice when compared with $Ppara^{+/+}$ mice, but statistical significance was lost when comparing to $Ppara^{\Delta Hep}$ mice, indicating an intermediate phenotype. PL levels were increased by fasting in $Ppara^{+/+}$ and $Ppara^{\Delta Hep}$ mice when compared with controls and unchanged in $Ppara^{-/-}$ mice (Fig. 4H). PL levels in fed animals were comparable. Circulating TG levels were

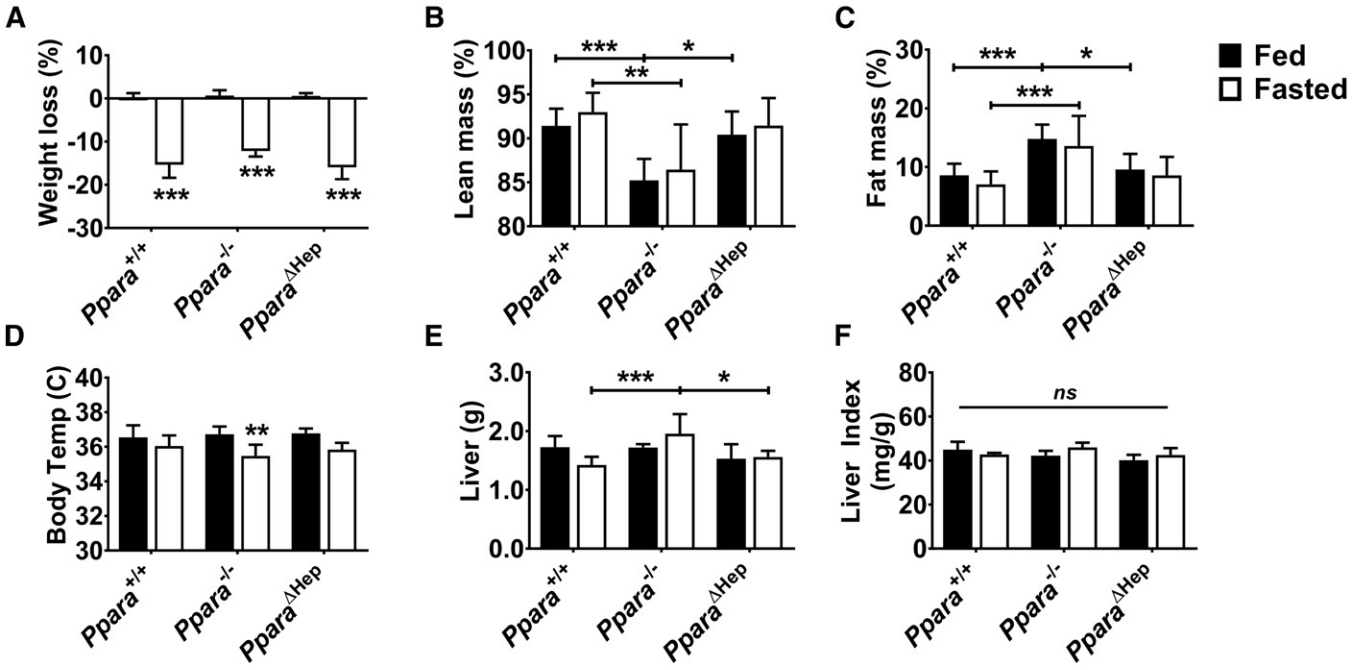

Fig. 1. Influence of *Ppara* status on physiological response to fasting. WT (*Ppara*$^{+/+}$), full-body *Ppara*-null (*Ppara*$^{-/-}$), and hepatocyte-specific *Ppara*-null (*Ppara*$^{\Delta Hep}$) mice fed al libitum or fasted for 24 h. Weight loss (A), lean body mass (B), fat mass (C), body temperature (D), liver weight (E), and liver index (F) of different genotypes in response to fasting. Data are mean ± SD (n = 5). Asterisks above bars indicate significance versus fed group of the same genotype. * $P < 0.05$; ** $P < 0.01$; *** $P < 0.001$; ns, not significant.

similar between *Ppara*$^{+/+}$ and *Ppara*$^{\Delta Hep}$ mice and unchanged by fasting. TG levels were significantly lowered by fasting in *Ppara*$^{-/-}$ mice (Fig. 4I).

Serum FFAs were more precisely measured in fasted mice by LC/MS. Several FA species were elevated in the serum of *Ppara*$^{-/-}$ and *Ppara*$^{\Delta Hep}$ mice after fasting (C16:0, C16:1, C18:1, C18:2, and C18:3) when compared with WT (**Fig. 5A**). Levels of C16:1 and C18:3 were considerably higher in *Ppara*$^{-/-}$, and several other FAs were unchanged by fasting or genotype (Fig. 5B). In general, the relative

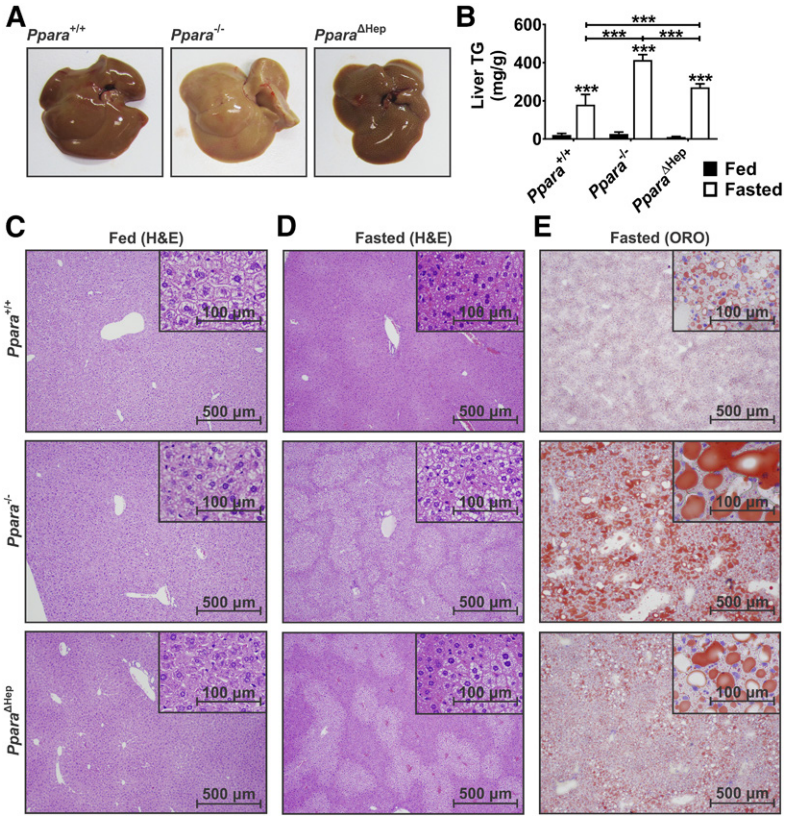

Fig. 2. Fasting-induced hepatosteatosis is exacerbated by PPARA ablation. WT (*Ppara*$^{+/+}$), full-body *Ppara*-null (*Ppara*$^{-/-}$), and hepatocyte-specific *Ppara*-null (*Ppara*$^{\Delta Hep}$) mice fed al libitum or fasted for 24 h. Gross liver physiology (A) and liver TG levels (B) after 24 h fast. H&E staining of sections from fed (C) and fasted (D) mouse livers. ORO staining (E) of fasted liver sections shows differential lipid accumulation. Data are mean ± SD (n = 5). Asterisks above bars indicate significance versus fed group of the same genotype. Representative images (n = 5) taken at 40× (scale bars = 500 mm) and 100× magnification (scale bars = 100 mm). *** $P < 0.001$.

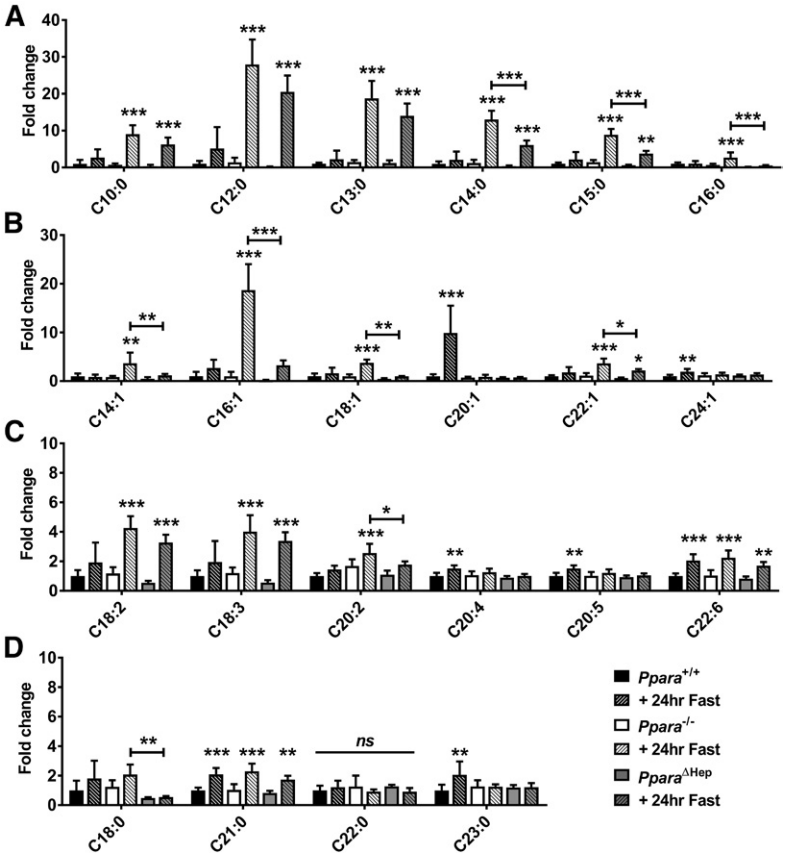

Fig. 3. Extrahepatic PPARA activity prevents accumulation of hepatic medium- to long-chain saturated FAs and MUFAs. FA levels were measured in livers of WT (*Ppara*$^{+/+}$), full-body *Ppara*-null (*Ppara*$^{-/-}$), and hepatocyte-specific *Ppara*-null (*Ppara*$^{\Delta Hep}$) mice by GC/MS. Saturated FAs (A), MUFAs (B), PUFAs (C), and longer-chain saturated FAs (D) were analyzed in fed and fasted states. Data are shown as mean fold change ± SD (n = 5) versus fed WT groups. Data represent peak area response normalized to total tissue weight. Asterisks above bars indicate significance versus fed group of the same genotype. * $P < 0.05$; ** $P < 0.01$; *** $P < 0.001$; ns, not significant.

levels of PUFAs were lower than MUFAs or saturated FAs (Fig. 5C). The release of FFAs from fat stores was coupled to the release of GLY. Serum GLY was therefore measured by GC/MS (Fig. 4E). GLY levels were only elevated in fasted *Ppara*$^{-/-}$ mice when compared with WT. GLY concentrations in *Ppara*$^{\Delta Hep}$ mice were not significantly different than either WT or *Ppara*$^{-/-}$ mice, demonstrating an intermediate phenotype. In vivo lipolysis experiments were also performed to assess adipose FA and GLY release, as well as utilization by tissues, using the β3-adrenoceptor agonist CL316243. Serum FFA and GLY response to CL316243 was comparable to fasted samples (supplemental Fig. S1). These data show that extrahepatic PPARA activity influences serum lipid profiles in fasted *Ppara*$^{\Delta Hep}$ mice. These differences could be the result of differential adipose mobilization or increased FA utilization by extrahepatic tissues. As such, the expression of genes involved in FA metabolism were assessed in extrahepatic tissues, and total lipase activity was measured to gauge FA mobilization.

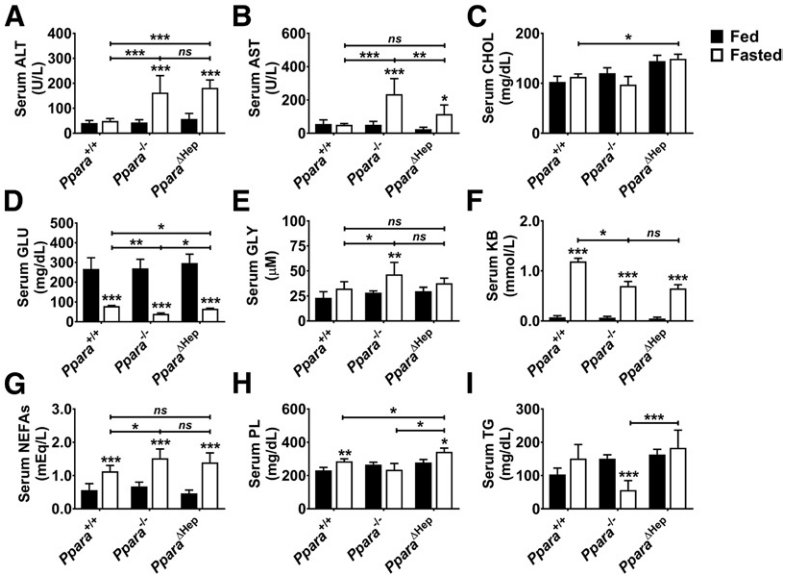

Fig. 4. Effect of *Ppara* status and acute fasting on serum chemistries. Mice were fed al libitum or fasted for 24 h, and then serum was collected for analysis. Serum ALT (A), AST (B), CHOL (C), GLU (D), GLY (E), KBs (F), NEFAs (G), PLs (H), and TGs (I) were measured. Data represent mean ± SD (n = 5). * $P < 0.05$; ** $P < 0.01$; *** $P < 0.001$; ns, not significant.

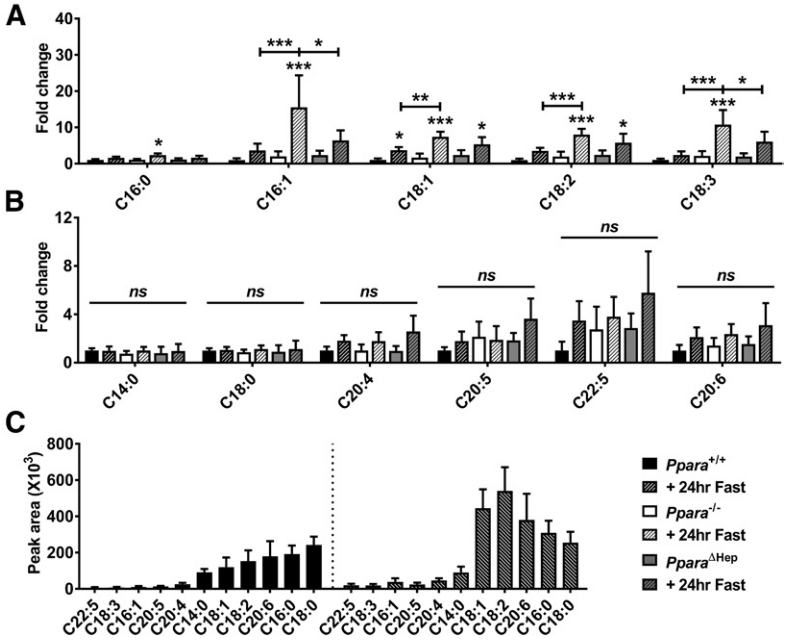

Fig. 5. Extrahepatic PPARA normalizes serum FA response in fasted *Ppara*$^{\Delta Hep}$ mice. Mice were fed ad libitum or fasted for 24 h, and then serum was collected for analysis. *Ppara*-dependent (A) and -independent (B) changes in serum FAs in fasted *Ppara*$^{+/+}$, full-body *Ppara*-null (*Ppara*$^{-/-}$), and hepatocyte-specific *Ppara*-null (*Ppara*$^{\Delta Hep}$) mice. C: Mean MS peak area data indicating relative abundance of individual FAs in fed and fasted WT (*Ppara*$^{+/+}$) mouse serum. Fold change data are shown as mean fold change ± SD (n = 5) versus fed WT groups. Asterisks above bars indicate significance versus fed group of the same genotype. * $P < 0.05$; ** $P < 0.01$; *** $P < 0.001$; ns, not significant.

Hepatic PPARA primarily controls FAO-related gene expression in response to fasting

Known PPARA target gene mRNAs, additional lipid metabolism-related mRNAs, and VLDL synthesis-related mRNAs were measured to identify factors that influence lipid accumulation and steatosis. "Classic" PPARA target gene expression associated with FAO [acyl-CoA dehydrogenase (*Acadm*); acyl-CoA dehydrogenase, long chain (*Acadl*); acyl-CoA oxidase 1 (*Acox1*); carnitine palmitoyltransferase 1b (*Cpt1b*); carnitine palmitoyltransferase 2 (*Cpt2*); and enoyl-CoA hydratase and 3-hydroxyacyl CoA dehydrogenase (*Ehhadh*)] was completely dependent on hepatocyte-specific PPARA activation (**Fig. 6A**). *Ppara* status differentially impacted several genes that are either directly or indirectly related to lipid homeostasis including cytochrome P450, family 2, subfamily b, polypeptide 9 (*Cyp2b9*); *Cyp8a1*; *Etppl*; lipocalin 2 (*Lcn2*); and lipocalin 13 (*Lcn13*) (Fig. 6B). CYP2B9 and cytochrome P450, family 8, subfamily b, polypeptide 1 (CYP8B1) are involved in steroid and bile acid synthesis, respectively. These two enzymes were upregulated in fasted *Ppara*$^{+/+}$ and *Ppara*$^{\Delta Hep}$ mice but not *Ppara*$^{-/-}$ mice. Ethanolamine-phosphate phospho-lyase (ETNPPL) is associated with glycerophospholipid metabolism, and fasting resulted in downregulation of *Etnppl* mRNA only in *Ppara*$^{-/-}$ mice. The lipocalins encoded by *Lcn2* and *Lcn13* bind and transport small hydrophobic molecules, including lipids. Similar to WT, fasting downregulated *Lcn2* and *Lcn13* mRNAs in *Ppara*$^{\Delta Hep}$ mice. Basal lipocalin (*Lcn*) mRNA expression was much lower in *Ppara*$^{-/-}$ mice and upregulated after fasting. Expression of *Lpl* was unaffected by treatment or genotype. An increase in hepatic TGs (Fig. 2B) and decrease in serum TGs (Fig. 4I) in *Ppara*$^{-/-}$ mice suggests that VLDL production may be impaired. Rate-limiting genes involved in VLDL production (*Apob*, *Apoc2*, and *Apoe*) and lipid import (*Cd36*, *Slc27a4*, and *Slc27a5*) were quantified (Fig. 6C). These mRNAs were not impacted by fasting or genotype, so VLDL production does not seem to be altered at the transcriptional level. Hepatic FAO associated mRNAs was similarly impaired in both *Ppara*$^{-/-}$ and *Ppara*$^{\Delta Hep}$ mice. Lipid accumulation is often coupled to oxidative stress and LPO (16). Several antioxidant response genes (*glutathione S-transferase α 2*, *glutathione S-transferase kappa 1*, and *glutathione S-transferase mu 3*) mRNAs were elevated only in *Ppara*$^{-/-}$ mice (supplemental Fig. S2A). Moreover, DCFDA and malondialdehyde (MDA) assays confirmed an increase in ROS and LPO, respectively, in the livers of *Ppara*$^{-/-}$ after a 24 h fast (supplemental Fig. S2B, C). Although several differentially expressed genes were identified, none mechanistically explain the pronounced difference in hepatosteatosis, indicating that extrahepatic tissues may play a compensatory role in lipid metabolism.

FAO is elevated in extrahepatic tissues of fasted *Ppara*$^{\Delta Hep}$ mice

The liver is often considered the primary site of lipid catabolism, but many extrahepatic tissues have significant oxidative capacity. Gene expression was measured in extrahepatic tissues to test whether a compensatory increase in FAO may protect against hepatosteatosis by reducing systemic lipid load. *Acadm*, *Cpt1b*, *Ehhadh*, fibroblast growth factor 21 (*Fgf21*), and pyruvate dehydrogenase kinase 4 (*Pdk4*) mRNAs were measured in BAT, heart, liver, and skeletal muscle from fed and fasted *Ppara*$^{+/+}$, *Ppara*$^{-/-}$, and *Ppara*$^{\Delta Hep}$ mice (**Fig. 7**). Fasting-induced PPARA-dependent upregulation of all genes in the livers of WT mice supported the hepatic FAO deficiency noted in *Ppara*$^{\Delta Hep}$ and *Ppara*$^{-/-}$ mice. Extrahepatic *Acadm*, *Cpt1b*, *Ehhadh*, and *Fgf21* mRNA expression was upregulated in fasted *Ppara*$^{+/+}$ as well as *Ppara*$^{\Delta Hep}$ mice. Fasted *Ppara*$^{\Delta Hep}$ mice exhibited significantly higher expression of *Cpt1b* and *Ehhadh* mRNA in BAT, *Acadm* and *Cpt1b* mRNA in heart, and *Acadm*, *Cpt1b*, and *Ehhadh* mRNAs in muscle when compared with fasted *Ppara*$^{+/+}$ mice. *Acadm*, *Cpt1b*, *Ehhadh*, and *Fgf21* mRNA

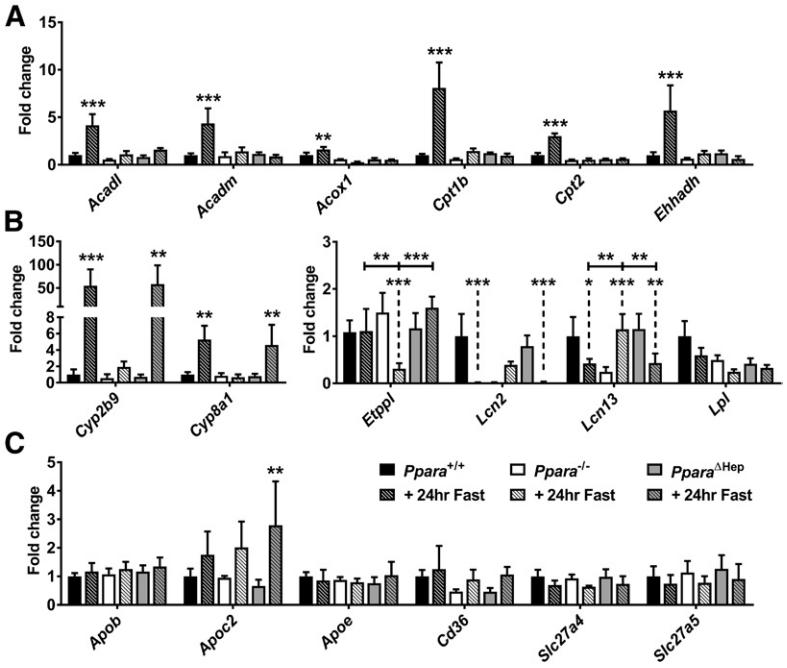

Fig. 6. Hepatic expression of lipid metabolism-related gene expression during fasting response. Mice were fasted for 24 h, and liver RNA was isolated for qRT-PCR analysis. Expression of β-oxidation (*Acadm*, *Acadl*, *Acox1*, *Cpt1b*, *Cpt2*, and *Ehhadh*) mRNAs (A) and lipid metabolism (*Cyp2b9*, *Cyp8b1*, *Etppl*, *Lcn2*, *Lcn13*, and *Lpl*) (B) related gene mRNAs. C: mRNAs encoded by hepatic genes involved in VLDL production (*Apob*, *Apoc2*, *Apoe*, and *Cd36*) and lipid transport (*Slc27a4* and *Slc27a5*). Data were normalized to *Actb* and expressed as fold change WT control. Data are mean ± SD (n = 5). Asterisks above bars indicate significance versus fed group of the same genotype. * $P < 0.05$; ** $P < 0.01$; *** $P < 0.001$.

expression was unchanged after fasting in *Ppara*$^{-/-}$, indicating that FAO is impaired in these tissues. *Pdk4* mRNA expression was elevated in all tissues but PPARA-dependent only in the liver, suggesting alternate regulatory mechanisms in other tissues. Elevated FAO in BAT, heart, and muscle of fasted *Ppara*$^{\Delta Hep}$ mice would reduce circulating lipids and potentially protect against hepatic lipid accumulation.

Total lipase activity is elevated in extrahepatic tissues of fasted *Ppara*$^{\Delta Hep}$ mice

Lipases are required for the mobilization of FAs from adipose depots as well as for the uptake of lipoprotein TGs into tissues. To test whether *Ppara* status influences lipid mobilization or uptake, total lipase activity was measured in inguinal white adipose tissue (IWAT), heart, liver, and

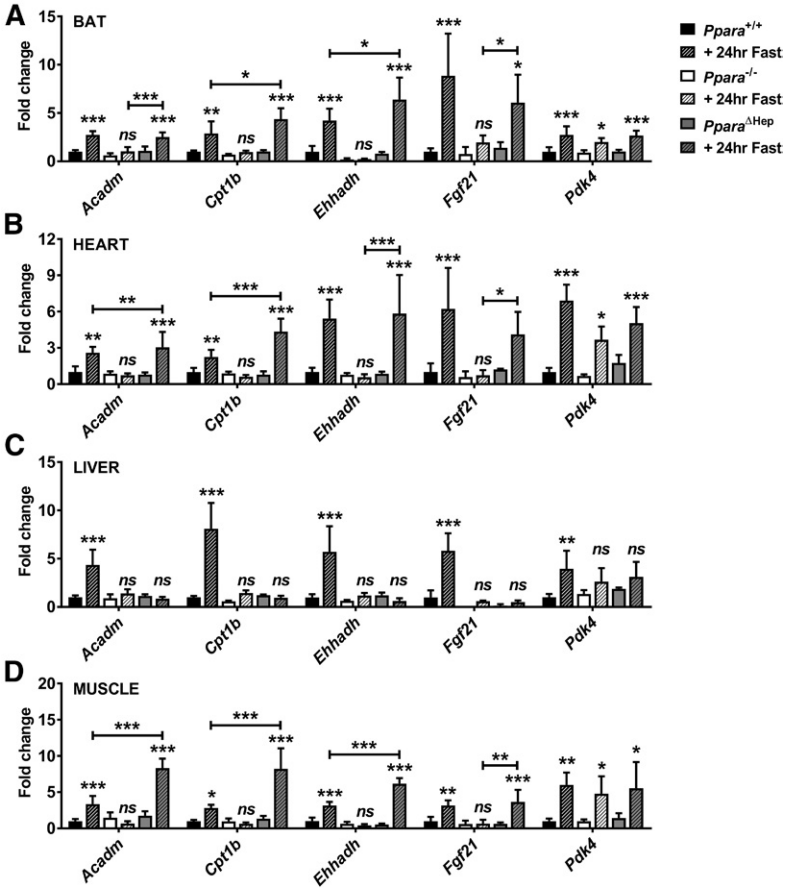

Fig. 7. FAO is elevated in extrahepatic tissues of fasted *Ppara*$^{\Delta Hep}$ mice. Mice were fasted for 24 h, and then tissues collected for RNA isolation and qRT-PCR analysis. Expression of PPARA target gene mRNAs involved in β-oxidation (*Acadm*, *Cpt1b*, and *Ehhadh*) and fasting response (*Fgf21* and *Pdk4*) were measured in BAT (A), heart (B), liver (C), and skeletal muscle (D). Data normalized to *Actb* and expressed as fold change WT control. Data are mean ± SD (n = 5). Asterisks above bars indicate significance versus fed group of the same genotype. * $P < 0.05$; ** $P < 0.01$; *** $P < 0.001$; ns, not significant.

skeletal muscle from fed and fasted mice (**Fig. 8**). Total lipase activity in IWAT increased comparably in all genotypes after a 24 h fast, indicating that adipose FA release was unaffected by *Ppara* status (Fig. 8A). This was supported by measurement of mRNAs associated with lipase (*Abhd5*, *Lipa*, *Lipe*, *Lpl*, *MglI*, and *Pnpla2*) in IWAT, BAT, and epididymal white adipose tissues (EWATs), which was not impacted by either fasting or genotype supporting FA mobilization from fat depots is comparable (supplemental Fig. S3). Cardiac total lipase activity was elevated by fasting in $Ppara^{+/+}$ and $Ppara^{\Delta Hep}$ mice (Fig. 8B). There was also a slight but significant increase lipase activity in fasted $Ppara^{\Delta Hep}$ mice when compared with WT mice, suggestive of enhanced cardiac lipid utilization. Total hepatic lipase activity increased slightly in both $Ppara^{+/+}$ and $Ppara^{\Delta Hep}$ mice after fasting (Fig. 8C). Interestingly, lipase activity in $Ppara^{-/-}$ mice was slightly but significantly elevated in fed mice when compared with $Ppara^{+/+}$ mice and decreased after a 24 h fast. Muscle lipase activity increased in all genotypes (Fig. 8D), but response was attenuated in $Ppara^{-/-}$ mice. To further characterize elevated extrahepatic lipase activity, *Abhd5*, *Lipa*, *Lipe*, *Lpl*, *Mgll*, and *Pnpla2* mRNAs levels were measured in heart and muscle. Cardiac *Lipe* and *Pnpla2* mRNA was increased over 3-fold in fasted $Ppara^{\Delta Hep}$ mice (**Fig. 9A**). *Abhd5*, *Lipa*, *Lpl*, and *Mgll* mRNAs did not respond to fasting. Muscle lipase expression was also not affected by feeding status (Fig. 9B). Elevated total lipase activity in heart and muscle of $Ppara^{\Delta Hep}$ mice combined with an increase in

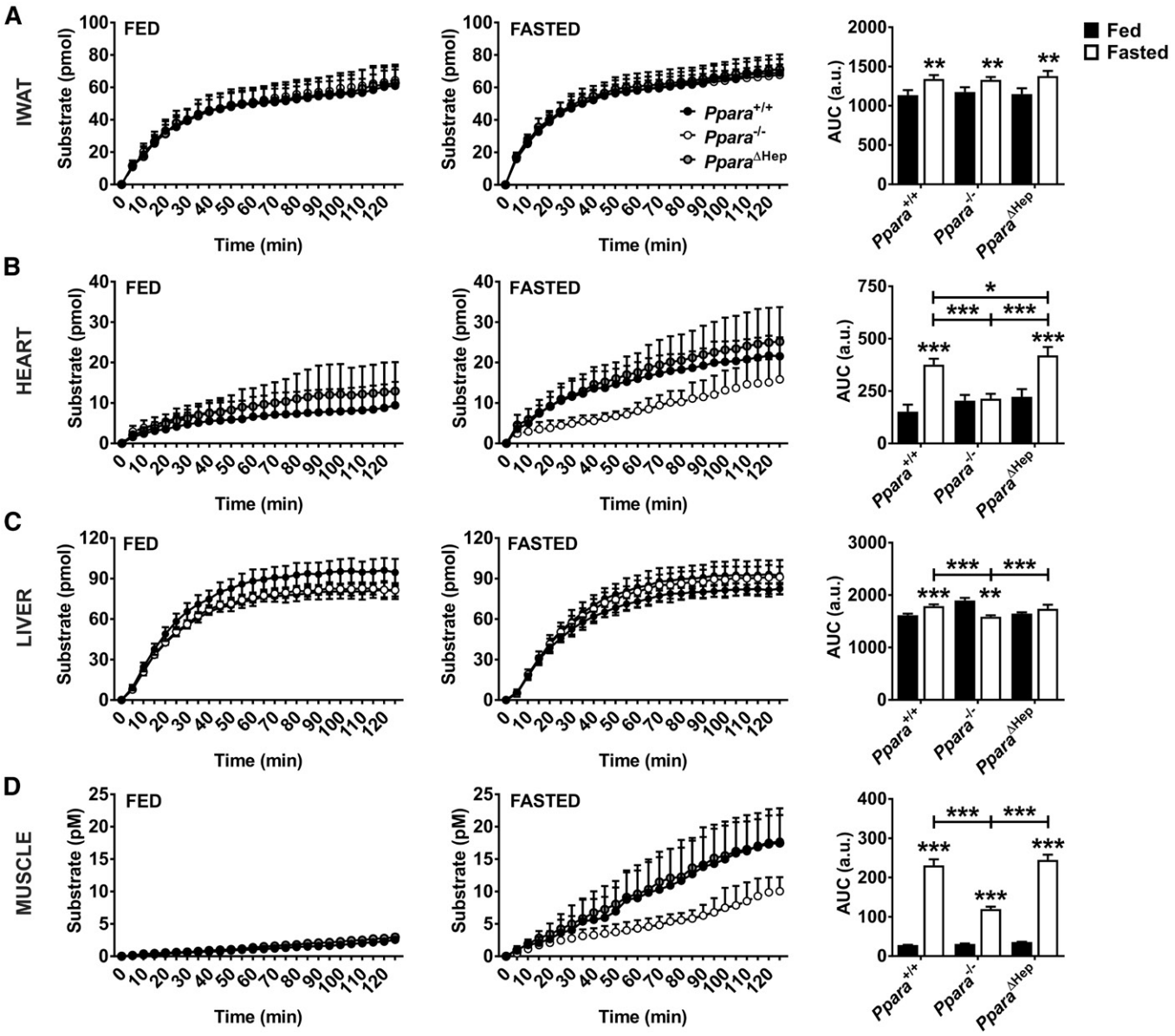

Fig. 8. Total lipase activity is elevated in extrahepatic tissues of fasted $Ppara^{\Delta Hep}$ mice. Mice were fasted for 24 h, and total lipase activity was measured in freshly isolated tissues. Lipase activity from inguinal inguinal white adipose tissue (IWAT) (A), heart (B), liver (C), and skeletal muscle (D) from $Ppara^{+/+}$, $Ppara^{-/-}$, and $Ppara^{\Delta Hep}$. Areas under the curve (AUCs) were calculated and tested for significance. Data are mean ± SD (n = 4–6). Asterisks above bars indicate significance versus fed group of the same genotype. a.u., arbitrary units. * $P < 0.05$; ** $P < 0.01$; *** $P < 0.001$.

FAO-related gene expression support an important role for PPARA during physiological response to fasting.

DISCUSSION

Studies utilizing *Ppara*$^{-/-}$ mice support PPARA as a key regulator of systemic lipid homeostasis in vivo. Fasted *Ppara*$^{-/-}$ mice are unable to properly catabolize mobilized lipids transported to the liver where they buildup, causing marked steatosis. Herein, *Ppara*$^{\Delta Hep}$ mice were shown to accumulate dramatically less hepatic lipid than *Ppara*$^{-/-}$ mice after a 24 h fast. Fasting caused a PPARA-dependent increase in FAO-related gene expression in BAT, heart, and skeletal muscle, total lipase activity in heart and muscle, and expression of cardiac lipase in *Ppara*$^{\Delta Hep}$ mice. These data confirm that PPARA is the primary regulator of FAO in extrahepatic tissues and show that nonhepatic FAO significantly contributes to systemic lipid utilization. Elevated FAO gene expression, lipase activity, and lipase expression would increase oxidative capacity and lipid catabolism, reduce lipid load, and prevent the steatosis and lipotoxicity observed in *Ppara*$^{-/-}$ mice. Hence, extrahepatic PPARA plays an important physiological role in peripheral tissues during food deprivation and attenuates fasting-induced hepatosteatosis in the absence of active hepatic PPARA. PPARA-dependent regulation of FAO within extrahepatic tissues would be of interest in the management and treatment of NASH and NAFLD patients, where accumulating evidence indicates that hepatic PPARA expression and activity are diminished.

PPARA plays a major role in regulating global lipid homeostasis. Other studies have assessed the role of PPARA during the fasting response with particular focus on the liver (17, 18). Interestingly, these studies are influenced by several factors, including fasting regimen, animal age, and diet, leading to inconsistencies in reproducibility between laboratories. Fasting regimens, for example, are often initiated at different times. PPARA expression has a diurnal rhythm in heart, liver, WAT, and BAT, but not muscle (19–21). Selecting the best time to begin a fasting study is complicated by the fact that peak *Ppara* expression is different for each tissue (20). Maximum *Ppara* mRNA expression in BAT, WAT, and liver are staggered by 4 h; therefore, endpoint collection times could significantly influence the resulting data. The impact of circadian rhythms on *Ppara* mRNA expression, PPARA protein levels, and PPARA activation potential in extrahepatic tissues and the resulting impact on lipid oxidation need to be explored further. Despite not fully understanding the role of PPARA in extrahepatic tissues, the importance of PPARA in lipid catabolism is manifested in higher adiposity noted in full-body *Ppara*-null mice (18, 22–24). WT and *Ppara*$^{\Delta Hep}$ mice had slightly lower body fat compositions, which need to be taken into consideration when assessing fasting-induced hepatosteatosis. However, weight loss between genotypes was similar, and the relative proportion of lean-to-fat mass was unaffected by fasting, suggesting that adipose tissue loss due to lipid mobilization was comparable. The present study also found that TGs in fasted *Ppara*$^{\Delta Hep}$ mice were unchanged and comparable to WT mice. Fasting caused serum TG levels to decrease in *Ppara*$^{-/-}$ mice. The drop in circulating TGs is coupled to a pronounced buildup of hepatic lipids and could be explained by impaired VLDL production in the liver. However, mRNA levels of genes required for VLDL production (*Apob*, *Apoc2*, and *Apoe*) were unaffected by genotype or fasting. Moreover, the expression of genes associated with FA import (*Cd36*, *Slc27a4*, and *Slc27a5*) were also unchanged. These data indicate that VLDL production is not altered at the transcriptional level. Interestingly, accumulation of FA substrates is known to impair VLDL assembly. Previous studies have revealed that medium-chain unsaturated FAs, such as decanoate (10:0) and dodecanoate (12:0), significantly decrease VLDL secretion (25, 26). A pronounced buildup of medium-chain unsaturated FAs was noted in fasted *Ppara*$^{-/-}$ when compared with *Ppara*$^{\Delta Hep}$. Inhibition of VLDL synthesis by medium unsaturated FA accumulation would decrease VLDL secretion and serum TGs, as well as exacerbate hepatosteatosis. Oxidative stress can also impair APO protein folding within the endoplasmic reticulum and subsequently prevent VLDL assembly (27). Experiments indicated that both ROS and LPO products were elevated in fasted *Ppara*$^{-/-}$ mice. The inhibition of VLDL synthesis by FA accumulation and oxidative stress would provide a mechanistic explanation for the observed difference in serum TG concentrations after fasting. Differences in other serum chemistries were minor. *Ppara*$^{\Delta Hep}$ mice displayed slightly higher serum CHOL, PLs, and TGs when compared with *Ppara*$^{-/-}$ mice, indicating that more lipids remain in circulation. Analysis of serum KBs revealed that levels were blunted in both knockout mouse models after fasting. These

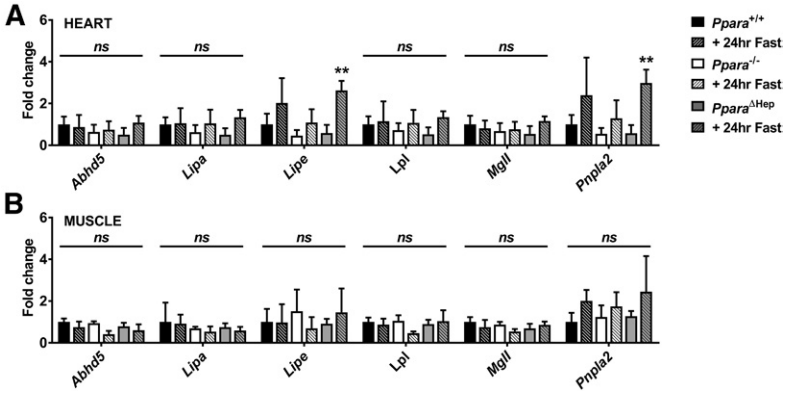

Fig. 9. Fasting upregulates cardiac *Lipe* and *Pnpla2* mRNAs in fasted *Ppara*$^{\Delta Hep}$ mice. Mice were fasted for 24 h, and then tissues were collected for RNA isolation and qRT-PCR analysis. Lipase-associated gene mRNAs (*Abhd5*, *Lipa*, *Lipe*, *Lpl*, *MglI*, and *Pnpla2*) were measured in heart (A) and muscle (B). Data were normalized to *Actb* and expressed as fold change WT control. Data are mean ± SD (n = 4–6). Asterisks above bars indicate significance versus fed group of the same genotype. ** $P < 0.01$; ns, not significant.

data demonstrate that hepatic PPARA promotes ketogenesis and that the contribution from extrahepatic tissues has a neglectable impact on circulating KB levels.

Fasting initiates the release of FAs from both adipose tissue and circulating lipoproteins, which are then transported to other tissues. The liver is often considered the primary site of lipid catabolism, and PPARA regulates FAO pathways. The present data revealed elevated lipids in livers from *Ppara*$^{-/-}$ and *Ppara*$^{\Delta Hep}$ mice, which were 2.5- and 1.5-fold higher than in WT mice, respectively. These data agree with another study that found differential TG accumulation in livers from *Ppara*$^{-/-}$ and *Ppara*$^{\Delta Hep}$ mice (18). The aim of the present study was to understand the underlying mechanisms responsible for the significant difference in pathology between these two mouse models. Although PPARA is primarily considered a hepatic nuclear receptor, the present study indicates that extrahepatic PPARA activity may contribute significantly to systemic lipid homeostasis. FAs are oxidized primarily by mitochondrial and peroxisomal β-oxidation. Short-chain FAs (SCFAs) and MCFAs are oxidized almost exclusively by mitochondrial β-oxidation. LCFAs are oxidized in both mitochondria and peroxisomes. A buildup of MCFAs and LCFAs was found in *Ppara*$^{-/-}$ and *Ppara*$^{\Delta Hep}$ models, suggesting that mitochondrial and peroxisomal β-oxidation are significantly impaired. PPARA status had less impact as FA length and degree of unsaturation increased. The expression of β-oxidation-related genes were upregulated in livers of fasted *Ppara*$^{+/+}$ mice and completely ablated in both *Ppara*$^{-/-}$ and *Ppara*$^{\Delta Hep}$ mice. The PPARA-dependent increase of FAO in extrahepatic tissues could provide an explanation for the differences in hepatic lipid accumulation. These studies suggest that FAO gene expression was elevated in tissues *1*) considered sites of FAO and *2*) express PPARA. Analysis of BAT, heart, and muscle confirmed the PPARA-dependent upregulation FAO-related mRNAs. Gene response was observed after fasting in *Ppara*$^{+/+}$ and *Ppara*$^{\Delta Hep}$ mice in all extrahepatic tissues tested but was completely absent in *Ppara*$^{-/-}$ mice. Furthermore, FAO genes were further upregulated in *Ppara*$^{\Delta Hep}$ mice when compared with WT mice, indicating that FAO gene expression can function as a compensatory mechanism for dealing with excess lipid load due to hepatic PPARA deficiency. These data provide convincing support that FAO is increased in these tissues and that fasting response in extrahepatic tissues is also controlled by PPARA.

Several hepatic genes were identified as differentially regulated in *Ppara*$^{-/-}$ and *Ppara*$^{\Delta Hep}$ mice. These genes are most likely expressed in nonparenchymal cells. Few studies have focused on PPARA function within other hepatic cell types, such as cholangiocytes, endothelial cells, Kupffer cells, or stellate cells, which play an important role in stress response and disease progression. Notably, *Cyp2b9* and *Cyp8b1* mRNAs were upregulated in fasted *Ppara*$^{+/+}$ and *Ppara*$^{\Delta Hep}$ mice, but not *Ppara*$^{-/-}$ mice. CYP2B9 is a constitutive androstane receptor-regulated testosterone hydroxylase, and its expression was found to decrease lipid peroxidation, suggesting that it may contribute to the lower MDA levels in *Ppara*$^{\Delta Hep}$ mice (28–30). CYP8B1 is an important player in bile acid metabolism, and its expression paralleled *Cyp2b9* mRNA, suggesting that PPARA may play important and unexplored role in bile acid metabolism. *Etnppl* mRNA was significantly downregulated in response to fasting only in *Ppara*$^{-/-}$ mice. A recent report found that *Etnppl* mRNA is downregulated in hepatocellular carcinoma patients and may function as an antilipogenesis protein (31). The *Lcn* protein family binds small hydrophobic molecules, including lipids. *Lcn2* plays an important role in control of cellular stress response; studies have supported protective effects in the liver, and expression is considered an indicator of liver damage (32, 33). *Lcn13* was recently found to encode a novel insulin sensitizer that protects against hepatosteatosis by inhibiting lipogenesis and inhibiting FAO (34, 35). *Lcn2* and *Lcn13* mRNA expression were suppressed in fasted *Ppara*$^{+/+}$ and *Ppara*$^{\Delta Hep}$ mice, whereas expression increased almost 40-fold in *Ppara*$^{-/-}$ mice. The exact function of these genes during fasting response is unknown, but the PPARA-dependent regulation of genes within nonparenchymal cells could represent novel elements of hepatic stress response and warrants further exploration.

The present data indicate that total lipase activity in oxidative extrahepatic tissues—namely, heart and skeletal muscle—was elevated in fasted *Ppara*$^{\Delta Hep}$ mice when compared with *Ppara*$^{-/-}$ mice and more closely corresponded to WT mice, demonstrating that PPARA expression plays an important role in lipid mobilization and utilization in these tissues. Moreover, cardiac total lipase activity in fasted *Ppara*$^{\Delta Hep}$ mice was higher than in *Ppara*$^{+/+}$ mice, supporting enhanced lipid utilization. Studies have shown that cardiac LPL activity increases almost 40% in rodents after a 24 h fast and may underlie the observed increase in total lipase activity (36, 37). There was a significant increase in total lipase activity in IWAT of all genotypes. Total lipase activity was comparable between groups, consistent with the view that adipose PPARA does not influence FA mobilization from adipose stores. The impact of fasting on the expression of adipose lipases were measured in IWAT, BAT, and EWAT. mRNA expression was unchanged in response to fasting in all adipose depots, indicating that regulation occurs independent of PPARA. This observation is supported by a recent study that found pharmacological PPARA activation had a minimal effect on the IWAT transcriptome in *Ppara*$^{-/-}$ mice (38). Lipase regulation is complex and involves transcriptional, translational, and posttranslational mechanisms, but regulation at all levels should be reflected in total lipase measurements. Therefore, lower levels of serum FFAs and GLY detected in *Ppara*$^{\Delta Hep}$ mice after fasting, and in response to CL316243, is most likely due to the PPARA-dependent uptake and utilization of lipids within nonhepatic tissues. The PPARA-dependent increase in FAO gene expression and total lipase activity in nonhepatic oxidative tissues such as heart, skeletal muscle, and BAT provides convincing evidence that metabolism of surplus lipid by extrahepatic tissues can protect against hepatic steatosis. PPARA expression is high in many oxidative tissues, including BAT, heart, and muscle. PPARA activation is highly dependent on ligand availability,

and it is thought that LCFAs serve as a principal endogenous PPARA ligand (39). During fasting, FAs are mobilized, and circulating levels increase. This study shows that serum LCFAs are significantly elevated in full-body *Ppara*-null mice and that liver-specific *Ppara*-null mice present an intermediate phenotype. The "compensatory" increase in PPARA target gene expression may be due to higher circulating ligands in the form of LCFAs in these mice. Moreover, unbound FAs released locally through VLDL lipolysis also act as PPARA ligands (40). The present data show an increase in cardiac lipase activity, which would further contribute to elevated PPARA ligand concentrations. Elevated ligand availability in peripheral tissues of liver-specific KO mice would be expected to increase PPARA activation and increase, as well as prolong, target gene expression. Another intriguing possibility is that other nuclear receptors contribute to peripheral gene expression and lipid metabolism in the absence of hepatic PPARA. Like PPARA, estrogen-related receptor α (ESRRA) is a nuclear receptor expressed at high levels in tissues that utilize FAO as an energy source. ESRRA is still referred to as an orphan receptor because no endogenous ligands have been identified to date, but studies have shown that it plays a role in cellular energetics by contributing to oxidative metabolism. Additional work is needed to fully understand the functional overlap of PPARA and other nuclear receptors during fasting response in hepatic and nonhepatic tissues.

In summary, this study provides evidence that extrahepatic PPARA activity significantly contributes to systemic response to prolonged fasting. The results indicate that the PPARA-dependent regulation of FAO in peripheral tissues can play a compensatory role when hepatic PPARA function is diminished and circulating lipids are elevated. Furthermore, PPARA-mediated FAO in nonhepatic tissues may have important clinical implications in patients with diseases associated with impaired hepatic PPARA function, such as NASH and NAFLD.

AlbCre mice were provided by Derek LeRoith at the Mount Sinai School of Medicine.

REFERENCES

1. Abdelmegeed, M. A., K. H. Moon, J. P. Hardwick, F. J. Gonzalez, and B. J. Song. 2009. Role of peroxisome proliferator-activated receptor-α in fasting-mediated oxidative stress. *Free Radic. Biol. Med.* **47:** 767–778.
2. Leone, T. C., C. J. Weinheimer, and D. P. Kelly. 1999. A critical role for the peroxisome proliferator-activated receptor α (PPARα) in the cellular fasting response: the PPARα-null mouse as a model of fatty acid oxidation disorders. *Proc. Natl. Acad. Sci. USA.* **96:** 7473–7478.
3. Kersten, S., J. Seydoux, J. M. Peters, F. J. Gonzalez, B. Desvergne, and W. Wahli. 1999. Peroxisome proliferator-activated receptor α mediates the adaptive response to fasting. *J. Clin. Invest.* **103:** 1489–1498.
4. Longo, V. D., and M. P. Mattson. 2014. Fasting: molecular mechanisms and clinical applications. *Cell Metab.* **19:** 181–192.
5. Francque, S., A. Verrijken, S. Caron, J. Prawitt, R. Paumelle, B. Derudas, P. Lefebvre, M. R. Taskinen, W. Van Hul, I. Mertens, et al. 2015. PPARα gene expression correlates with severity and histological treatment response in patients with non-alcoholic steatohepatitis. *J. Hepatol.* **63:** 164–173.
6. Ahrens, M., O. Ammerpohl, W. von Schonfels, J. Kolarova, S. Bens, T. Itzel, A. Teufel, A. Herrmann, M. Brosch, H. Hinrichsen, et al. 2013. DNA methylation analysis in nonalcoholic fatty liver disease suggests distinct disease-specific and remodeling signatures after bariatric surgery. *Cell Metab.* **18:** 296–302.
7. Dharancy, S., M. Malapel, G. Perlemuter, T. Roskams, Y. Cheng, L. Dubuquoy, P. Podevin, F. Conti, V. Canva, D. Philippe, et al. 2005. Impaired expression of the peroxisome proliferator-activated receptor α during hepatitis C virus infection. *Gastroenterology.* **128:** 334–342.
8. Zhang, J., Y. Zhao, C. Xu, Y. Hong, H. Lu, J. Wu, and Y. Chen. 2014. Association between serum free fatty acid levels and nonalcoholic fatty liver disease: a cross-sectional study. *Sci. Rep.* **4:** 5832.
9. de Almeida, I. T., H. Cortez-Pinto, G. Fidalgo, D. Rodrigues, and M. E. Camilo. 2002. Plasma total and free fatty acids composition in human non-alcoholic steatohepatitis. *Clin. Nutr.* **21:** 219–223.
10. Kersten, S., and R. Stienstra. 2017. The role and regulation of the peroxisome proliferator activated receptor α in human liver. *Biochimie.* **136:** 75–84.
11. Mukherjee, R., L. Jow, D. Noonan, and D. P. McDonnell. 1994. Human and rat peroxisome proliferator activated receptors (PPARs) demonstrate similar tissue distribution but different responsiveness to PPAR activators. *J. Steroid Biochem. Mol. Biol.* **51:** 157–166.
12. Lee, S. S., T. Pineau, J. Drago, E. J. Lee, J. W. Owens, D. L. Kroetz, P. M. Fernandez-Salguero, H. Westphal, and F. J. Gonzalez. 1995. Targeted disruption of the α isoform of the peroxisome proliferator-activated receptor gene in mice results in abolishment of the pleiotropic effects of peroxisome proliferators. *Mol. Cell. Biol.* **15:** 3012–3022.
13. Brocker, C. N., J. Yue, D. Kim, A. Qu, J. A. Bonzo, and F. J. Gonzalez. 2017. Hepatocyte-specific PPARA expression exclusively promotes agonist-induced cell proliferation without influence from nonparenchymal cells. *Am. J. Physiol. Gastrointest. Liver Physiol.* **312:** G283–G299.
14. Bustin, S. A., V. Benes, J. Garson, J. Hellemans, J. Huggett, M. Kubista, R. Mueller, T. Nolan, M. W. Pfaffl, G. Shipley, et al. 2013. The need for transparency and good practices in the qPCR literature. *Nat. Methods.* **10:** 1063–1067.
15. Pfaffl, M. W. 2001. A new mathematical model for relative quantification in real-time RT-PCR. *Nucleic Acids Res.* **29:** e45.
16. Bellanti, F., R. Villani, A. Facciorusso, G. Vendemiale, and G. Serviddio. 2017. Lipid oxidation products in the pathogenesis of non-alcoholic steatohepatitis. *Free Radic. Biol. Med.* **111:** 173–185.
17. Régnier, M., A. Polizzi, Y. Lippi, E. Fouché, G. Michel, C. Lukowicz, S. Smati, A. Marrot, F. Lasserre, C. Naylies, et al. 2018. Insights into the role of hepatocyte PPARα activity in response to fasting. *Mol. Cell. Endocrinol.* **471:** 75–88.
18. Montagner, A., A. Polizzi, E. Fouche, S. Ducheix, Y. Lippi, F. Lasserre, V. Barquissau, M. Regnier, C. Lukowicz, F. Benhamed, et al. 2016. Liver PPARα is crucial for whole-body fatty acid homeostasis and is protective against NAFLD. *Gut.* **65:** 1202–1214.
19. Lemberger, T., R. Saladin, M. Vazquez, F. Assimacopoulos, B. Staels, B. Desvergne, W. Wahli, and J. Auwerx. 1996. Expression of the peroxisome proliferator-activated receptor α gene is stimulated by stress and follows a diurnal rhythm. *J. Biol. Chem.* **271:** 1764–1769.
20. Yang, X., M. Downes, R. T. Yu, A. L. Bookout, W. He, M. Straume, D. J. Mangelsdorf, and R. M. Evans. 2006. Nuclear receptor expression links the circadian clock to metabolism. *Cell.* **126:** 801–810.
21. Wu, X., Z. Liu, G. Shi, L. Xing, X. Wang, X. Gu, Z. Qu, Z. Dong, J. Xiong, X. Gao, et al. 2011. The circadian clock influences heart performance. *J. Biol. Rhythms.* **26:** 402–411.
22. Knauf, C., J. Rieusset, M. Foretz, P. D. Cani, M. Uldry, M. Hosokawa, E. Martinez, M. Bringart, A. Waget, S. Kersten, et al. 2006. Peroxisome proliferator-activated receptor-α-null mice have increased white adipose tissue glucose utilization, GLUT4, and fat mass: role in liver and brain. *Endocrinology.* **147:** 4067–4078.
23. Guerre-Millo, M., C. Rouault, P. Poulain, J. Andre, V. Poitout, J. M. Peters, F. J. Gonzalez, J. C. Fruchart, G. Reach, and B. Staels. 2001. PPAR-α-null mice are protected from high-fat diet-induced insulin resistance. *Diabetes.* **50:** 2809–2814.
24. Peters, J. M., Y. Park, F. J. Gonzalez, and M. W. Pariza. 2001. Influence of conjugated linoleic acid on body composition and target gene expression in peroxisome proliferator-activated receptor α-null mice. *Biochim. Biophys. Acta.* **1533:** 233–242.
25. Sato, K., Y. Cho, S. Tachibana, T. Chiba, W. J. Schneider, and Y. Akiba. 2005. Impairment of VLDL secretion by medium-chain fatty

acids in chicken primary hepatocytes is affected by the chain length. *J. Nutr.* **135:** 1636–1641.
26. Sundaram, M., and Z. Yao. 2010. Recent progress in understanding protein and lipid factors affecting hepatic VLDL assembly and secretion. *Nutr. Metab. (Lond.).* **7:** 35.
27. Liu, M., S. Chung, G. S. Shelness, and J. S. Parks. 2012. Hepatic ABCA1 and VLDL triglyceride production. *Biochim. Biophys. Acta.* **1821:** 770–777.
28. Pham, M. H., H. Rhinn, N. Auzeil, A. Regazzetti, D. E. Harami, D. Scherman, and G. G. Chabot. 2011. Identification and induction of cytochrome P450s involved in the metabolism of flavone-8-acetic acid in mice. *Drug Metab. Lett.* **5:** 73–84.
29. Udomsuk, L., T. Juengwatanatrakul, W. Putalun, and K. Jarukamjorn. 2012. Bimodal action of miroestrol and deoxymiroestrol, phytoestrogens from *Pueraria candollei var. mirifica*, on hepatic CYP2B9 and CYP1A2 expressions and antilipid peroxidation in mice. *Nutr. Res.* **32:** 45–51.
30. Cho, H. Y., J. Y. Jung, H. Park, J. Y. Yang, S. Jung, J. H. An, S. W. Cho, S. W. Kim, S. Y. Kim, J. E. Kim, et al. 2014. In vivo deletion of CAR resulted in high bone mass phenotypes in male mice. *J. Cell. Physiol.* **229:** 561–571.
31. Ding, Q., J. Kang, J. Dai, M. Tang, Q. Wang, H. Zhang, W. Guo, R. Sun, and H. Yu. 2016. AGXT2L1 is down-regulated in heptocellular carcinoma and associated with abnormal lipogenesis. *J. Clin. Pathol.* **69:** 215–220.
32. Asimakopoulou, A., E. Borkham-Kamphorst, M. Henning, E. Yagmur, N. Gassler, C. Liedtke, T. Berger, T. W. Mak, and R. Weiskirchen. 2014. Lipocalin-2 (LCN2) regulates PLIN5 expression and intracellular lipid droplet formation in the liver. *Biochim. Biophys. Acta.* **1842:** 1513–1524.
33. Cai, Y., A. Jogasuria, H. Yin, M. J. Xu, X. Hu, J. Wang, C. Kim, J. Wu, K. Lee, B. Gao, et al. 2016. The detrimental role played by lipocalin-2 in alcoholic fatty liver in mice. *Am. J. Pathol.* **186:** 2417–2428.
34. Cho, K. W., Y. Zhou, L. Sheng, and L. Rui. 2011. Lipocalin-13 regulates glucose metabolism by both insulin-dependent and insulin-independent mechanisms. *Mol. Cell. Biol.* **31:** 450–457.
35. Sheng, L., K. W. Cho, Y. Zhou, H. Shen, and L. Rui. 2011. Lipocalin 13 protein protects against hepatic steatosis by both inhibiting lipogenesis and stimulating fatty acid β-oxidation. *J. Biol. Chem.* **286:** 38128–38135.
36. Trent, C. M., S. Yu, Y. Hu, N. Skoller, L. A. Huggins, S. Homma, and I. J. Goldberg. 2014. Lipoprotein lipase activity is required for cardiac lipid droplet production. *J. Lipid Res.* **55:** 645–658.
37. Ladu, M. J., H. Kapsas, and W. K. Palmer. 1991. Regulation of lipoprotein lipase in adipose and muscle tissues during fasting. *Am. J. Physiol.* **260:** R953–R959.
38. Defour, M., W. Dijk, P. Ruppert, E. B. M. Nascimento, P. Schrauwen, and S. Kersten. 2018. The peroxisome proliferator-activated receptor α is dispensable for cold-induced adipose tissue browning in mice. *Mol. Metab.* **10:** 39–54.
39. Nakamura, M. T., B. E. Yudell, and J. J. Loor. 2014. Regulation of energy metabolism by long-chain fatty acids. *Prog. Lipid Res.* **53:** 124–144.
40. Ruby, M. A., B. Goldenson, G. Orasanu, T. P. Johnston, J. Plutzky, and R. M. Krauss. 2010. VLDL hydrolysis by LPL activates PPAR-α through generation of unbound fatty acids. *J. Lipid Res.* **51:** 2275–2281.